TRANSPIRATION COOLING FILM EFFECTIVENESS CORRELATIONS FOR TURBINE BLADE APPLICATIONS

A. Wambersie – P.T. Ireland

Department of Engineering Science, University of Oxford
Oxford OX1 3PJ, UK
Email: augustin.wambersie@eng.ox.ac.uk

ABSTRACT

High porosity film cooling features have demonstrated exceptionally high film cooling performance. However, conventional methods to predict film cooling effectiveness have proved inaccurate for this new class of film. The inaccuracy is particularly true on the suction surface of the aerofoil where film effectiveness significantly exceeds predictions made using conventional correlations. RANS CFD simulations are equally limited beyond the immediate film hole region and generally over-predict the rate of film decay.

A novel approach to correlating these films is attempted in this paper using the similarities between tangential slot cooling distributions and existing experimental film data of porous cooling features. Based on this similarity, a correlation is developed by combining superposition with existing tangential slot injection models.

The success of this model reinforces both the premise that tangential slots and transpiration cooling share similar film distributions, as well as the hypothesis that the high porosity geometries proposed successfully mimic transpiration cooling.

KEYWORDS

FILM EFFECTIVENESS, PSP, TRANSPIRATION COOLING, HIGH POROSITY

NOMENCLATURE

c_p	Heat capacity (J/kgK)
C_1, C_2	Coefficients for Equation 9
d	Film hole diameter (m)
h	Heat transfer coefficient (W/m^{2}K)
M	Blowing ratio (
$\dot{m}_c$	Coolant mass flow rate (kg/s)
L	Characteristic length (m)
Pr	Prandtl number
Re	Reynolds number
T	Temperature (K)
U	Velocity (m/s)
x	Streamwise distance from film hole (m)
y	Spanwise distance (m)
α	Streamwise injection angle (°)
μ	dynamic viscosity (kg/ms)
η	Film effectiveness
$_{aw}$	Adiabatic wall condition
$_c$	Coolant
$_\infty$	Mainstream

INTRODUCTION

Recent experimental results have demonstrated the exceptional performance of high porosity cooling features on turbine blades (Wambersie et al. 2021). These highly effective geometries, rely on arrays of tightly packed film holes with small pitch to diameter ratios of around 2. The local surface porosity within the film hole arrays, defined as the fraction of the outer blade surface approaches 20%. The individual film holes operate at very low blowing ratios, defined in Equation 1, minimizing any penetration of the film intro the mainstream as well as the resultant mixing between the two gas streams. However, efforts to match these results to existing models, both analytical and numerical, has proven unsuccessful.

$$M = \frac{\rho_c \mathrm{u}_c}{\rho_\infty \mathrm{u}_\infty} \tag{1}$$

The ability to predict the film effectiveness, defined by Equation 2, of high porosity cooling features would allow for the evaluation of potential usefulness and impact of this technology.

This paper investigates film effectiveness distributions using both 1D and 2D models as a framework. Whilst the use of 1D models is limited within turbine blade applications due to geometric constraints, these nonetheless help demonstrate the overarching trend of high porosity films. The use of 2D models, by comparison, offers a more accurate approach which can be used to develop meaningful correlations. Nonetheless, both offer a great deal of qualitative understanding of cooling films developed using high porosity features.

$$\eta = \frac{T_\infty - T_{aw}}{T_\infty - T_c} \tag{2}$$

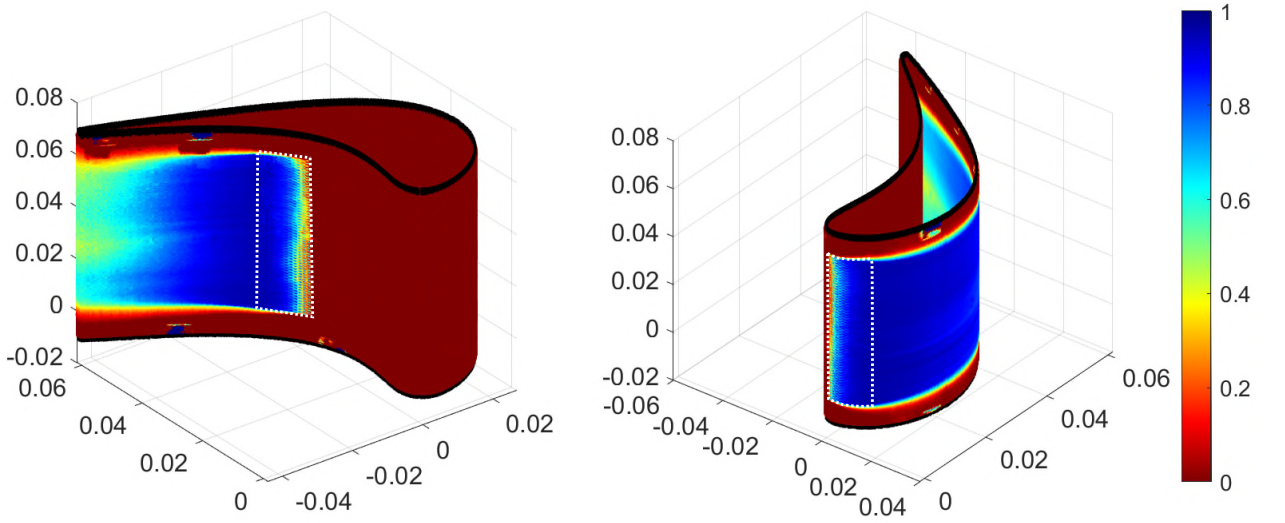

Figure 1 Demonstration of film effectiveness data obtained with a high porosity panel using 12.5g/s (1.5% of the mainstream) of coolant on both the pressure surface (left) and suction surface (right). Panels are outlined in white. (Wambersie, Ireland and Mayo 2021).

Several features of the films generated by high porosity panels, as illustrated by Figure 1, deserve particular attention and are summarized here. Moreover, these features serve as the catalyst for this investigation as a whole. The figure illustrates data for both a pressure surface and a suction surface panel geometry, tested within a highspeed cascade with a mainstream mass flow rate of 1.2kg/s. Firstly, the region immediately downstream of the film hole arrays demonstrates a near uniform level of film effectiveness. This is followed by a region of exponential-like decay further away from the point of coolant injection. The region of constant film effectiveness mimics the behavior of tangential slot injections studies, where the region with constant film effectiveness levels of unity is called the core region (Sturgess 1986). Across both experimental parametric studies on high porosity film arrays

as well as in tangential slot injection literature, the length and mean effectiveness of this core region were seen to be a clear function of the injection geometry. Conversely, the film effectiveness levels close to the trailing edge indicated almost no relationship with the injection geometry suggesting a breakdown in core structure and a return to a conventional mixed out boundary layer where film effectiveness is determined predominantly by the mass balance between injected coolant and hot mainstream gas that has been entrained into the boundary layer. Once again, this behavior draws parallels with previous work on tangential slot injection and its different zones (Simon 1986) .

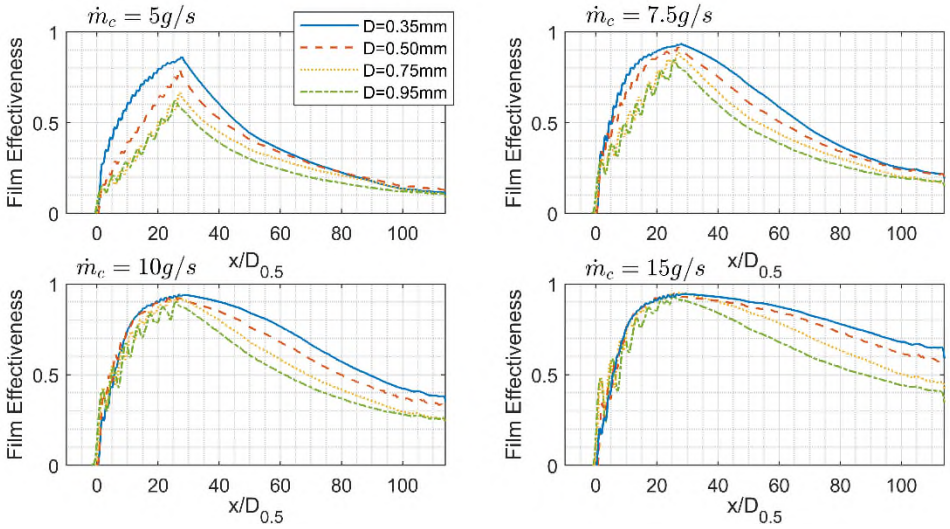

Figure 2 Demonstration of the effect of cooling hole diameter on film effectiveness levels at four different mass flow rates for a pressure surface geometry (Wambersie, Ireland and Mayo 2021)

Figure 2 exemplifies these parallels by plotting the film effectiveness of a series of high porosity panels of varying hole diameters. Film effectiveness levels are seen to converge towards the same values at the trailing edge, particularly at lower mass flow rates. As mass flow is increased, film effectiveness levels begin to diverge and then converge. Finally, the film begins to maintain near constant film effectiveness at 15g/s, particularly for smaller mass flows. This trend is only exacerbated at even higher mass flows.

To summarise, the film effectiveness distribution of recent experimental campaigns have pointed towards the need of a new method of predicting film effectiveness by drawing on parallels between these results and previous tangential slot injection studies.

LITERATURE REVIEW

1D film cooling models

1D film cooling models offer the most basic approach to predicting film effectiveness. Extensively studied and summarised by Goldstein (1971), 2D film correlations are based on a heat balance analogy within the boundary layer between the injected coolant and the entrained mainstream, with coolant simply acting as a heat sink and diluting the enthalpy of the boundary layer Using empirical boundary layer correlations to quantify the temperature profiles as well as entrainment rates, Equation 3 was developed.

$$\eta = \frac{1.9\mathrm{Pr}^{2/3}}{1+0.329\left(\frac{C_{p\infty}}{C_{pc}}\right)\varepsilon^{0.8}\beta} \tag{3}$$

Where ε is the dimensionless film cooling parameter with Re_2 and s representing the film hole Reynolds number slot height respectively.

$$\varepsilon = \left(\frac{x}{sM}\right)\left[\frac{\mu_c}{\mu_\infty} Re_2\right]^{-0.25} \quad (4)$$

And β is taken as the increase in the rate of entrainment into the boundary layer due to coolant injection.

$$\beta = 1 + 1.5 \times 10^{-4} Re_2 \frac{\mu_c}{\mu_\infty} \sin\alpha \quad (5)$$

Equation 3 was seen by Goldstein and Haji-Sheikh to closely correlate flat plate data of both porous sections as well as tangential slot injections where ***s*** refers to either the porous section length or the slot height.

Tangential slot models

Other approaches have been used to specifically correlate tangential slot injection films as these can demonstrate different film cooling distributions, particularly at high blowing ratios.

Sturgess (1986) suggests using a model in which the film can be categorized into three separate regions. The first is the potential core, where film effectiveness levels are effectively maintained at unity. This is followed by a region of decaying film effectiveness known as the wall jet region, where the boundary layer is still dominated by the coolant injection. This region slowly narrows towards the wall as mixing propagates from the interface between coolant and mainstream gas. Finally, the film becomes developed as the boundary layer mixes out completely, at which stage film cooling effectiveness is seen to match the standard heat sink film cooling models. Equation 6 describes the overall form of the film effectiveness where x_p is the length of the film core with film effectiveness values of unity given for $x < x_p$. MIX_n is defined as a function of the injection geometry.

$$\eta = f\left[\frac{(x-x_p)}{s\bar{M}}, MIX_n\right] \quad (6)$$

Velocity ratio, density ratio, and slot geometry are seen to have important effects on the core length. Simon (1986) similarly categorizes the film into two separate zones with a core and developed region and quantifies the effects of turbulence on the core length.

Hatch and Papell (1959) suggest an alternative approach to modeling tangential slot injections by using a different physical analogy. The mainstream and coolant stream are assumed to remain separate, with the heat transfer between the two driven by a characteristic HTC as shown in Equation 7. x' is given as the distance travelled by the coolant before heat is able to conduct through the coolant layer. Additional functions to fit the model to varying velocity ratios and injection angles are also included later in subsequent studies (Papell 1960).

$$\eta = \exp\left[-\left(\frac{hL(x-x')}{\dot{m}c_p}\right)\right] \quad (7)$$

Goldstein (1965) also noted that this approach provides a relatively accurate fit for transpiration sections as well as for tangential slots, indicating that models developed for either type of geometry could be interchanged within reason. However, these models were seen to be less effective beyond non dimensional streamwise distances with x/ML >100.

2D models

When modelling cooling features with multiple injection locations, the standard analytical approach involves modelling each individual film hole and superimposing the separate streams using the method defined by Sellers (1963). This approach has the benefit of being extremely simple and relatively accurate for most use cases. An improvement on this approach proposed by Kirollos and Povey (2015) that corrects the energy imbalance however the overall approach remains similar.

$$\eta = 1 - \prod_{i=1}^{n_{holes}} (1 - \eta_i) \tag{8}$$

Equation 8 can be applied in both streamwise and spanwise directions making it ideal for large banks of individual film holes. This approach also has the benefit of being able to model in between film holes as opposed to solely downstream of the overall feature. The film effectiveness of individual cylindrical film holes can be modelled in 2D as heat sinks using Equation 9 (Goldstein 1971) where y_h and x_{decay} are constants that are functions of blowing ratio. This approach has been demonstrated by Murray (2018)and Coulton who also suggested improvements to the spanwise distribution term (Coulton, Murray and Ireland 2022).

$$\eta = \frac{\mathrm{M\,U_\infty d}}{8\alpha(x/D + x_{decay})} \exp - \left(0.693 \frac{y}{y_h}\right)^2 \tag{9}$$

Note that this approach provides a local effectiveness that depends on both x and y. This method proves to be a highly effective and efficient approximation for flat plate geometries with pitch-to-diameter ratios of over ten in the streamwise direction. The constraint of large streamwise spacing allows the boundary layer to recover to a uniform velocity distribution and for the vortices developed by the interactions between film and mainstream to begin to dissipate. High blowing ratios increase this distance further as the impact on the boundary layer is more significant.

However, when pitch to diameter ratios are reduced to the order of 2-3, the interactions between films become significant and large variations in individual film behavior can be observed. Chen et al. (2020) demonstrated the potential discrepancies between film superposition and experiments in which two rows are positioned inline with pitch to diameter ratios. Whilst the standard film models can be tuned in an attempt to capture some of these effects, these still fall short when applied to either curved geometries in representative engine flows or when applied to high blowing ratio (BR) films that would typically lift off altogether if not for interactions with other films (Jiang, et al. 2018).

Long-standing similarities between the behaviors of tangential injection and transpiration cooling have been discussed. Multiple different approaches to modeling these geometries have also been presented, however, these have yet to be used successfully to predict the film effectiveness of high porosity film cooling features on real turbine blade geometries.

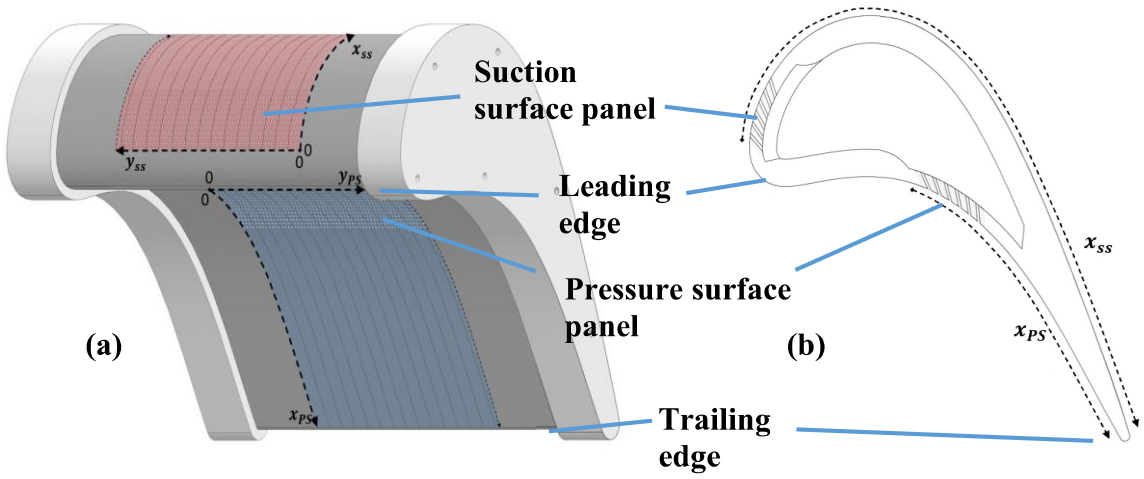

Figure 3 Schematic of geometries and locations used in film effectiveness experiments

Overview of film effectiveness data and geometries

Film effectiveness data from a wide range of high porosity panel geometries illustrated by Figure 1 is used to develop and test the correlations. The experimental setup as well as the initial set of results are detailed by Wambersie, Ireland and Mayo (2021) but have since been greatly expanded to include a much larger range of variables, including film hole diameter and panel length. Both the blowing

ratio and density ratio are also varied. The results offer high spatial resolution film effectiveness, though this paper will emphasize the streamwise distribution of film effectiveness as this has been the primary area of interest of these geometries, with the spanwise distribution being relatively uniform.

Whilst both inline and staggered geometry data is available, it was determined that film effectiveness data of inline geometries would not be particularly suitable to model as these films are exacerbated by film lift off. By comparison, staggered rows resulted in a much more robust, attached, and uniform films at all blowing ratios. A critical requirement for the geometries evaluated is that the films are closely packed together with a pitch to diameter ratio close to 2. This results in a feature where the bulk film of the panel array takes on a different distribution relative to that of the individual films.

2D FILM EFFECTIVENESS INVESTIGATION

Figure 4 demonstrates how the films generated by high porosity features scale with blowing ratio once the abscissa is offset by a potential core. As the film effective levels do not begin at unity, the length of the potential core was estimated as the distance between the panel trailing edge and the inflection point of the film effectiveness which could be systematically determined.

Equation 3 is also included for reference with the geometries modelled as porous sections with no offset, demonstrating that past a core or transitional region, the films behave predictably once the boundary layer temperature profile becomes developed and mixed out.

This would suggest that given a long enough surface, transpiration panels can be modelled simply as single porous geometries on flat plates with a streamwise offset. Figure 5, taken from a geometry on the late suction surface offers a visible representation of the core region as the values of film effectiveness at different mass flows diverge near the cooling geometry and then converge towards Equation 4. This indicates that there is an additional sensitivity to mass flow near the film holes not captured in the original correlation for the geometries being examined.

However, due to the length of a turbine blade geometry, a significant region of the relevant blade surface remains upstream of the predictable developed film regime for both suction and pressure surfaces. This is particularly true at higher mass flows where the core region extends almost to the trailing edge. Furthermore, the apparent length of the film core stemming from the early suction surface geometries exceeds the blade length altogether, rendering this approach useless for this region of the blade.

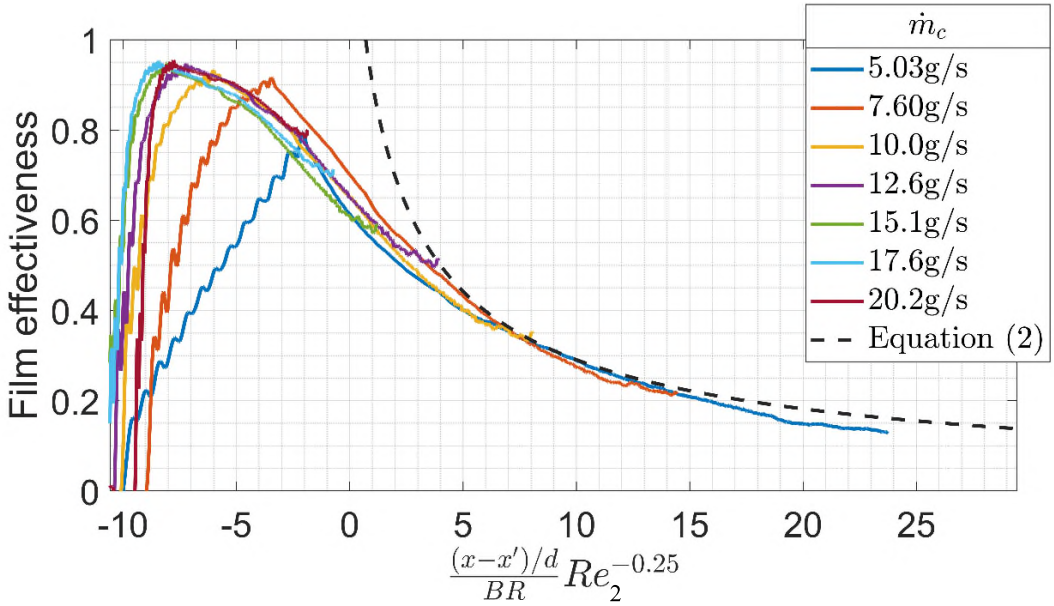

Figure 4 Film effectiveness levels plotted against scaled streamwise distance with core offset for 12 row staggered geometry on mid Pressure surface. (Wambersie, Ireland and Mayo 2021)

Overall, it can be concluded that the high porosity panels are able to develop a robust and sufficiently thick layer of coolant such that the effects of boundary layer entrainment are delayed until the boundary layer becomes fully mixed out. The potential core length is predominantly a function of the velocity ratio, however, mass flow and blade curvature also play a significant role.

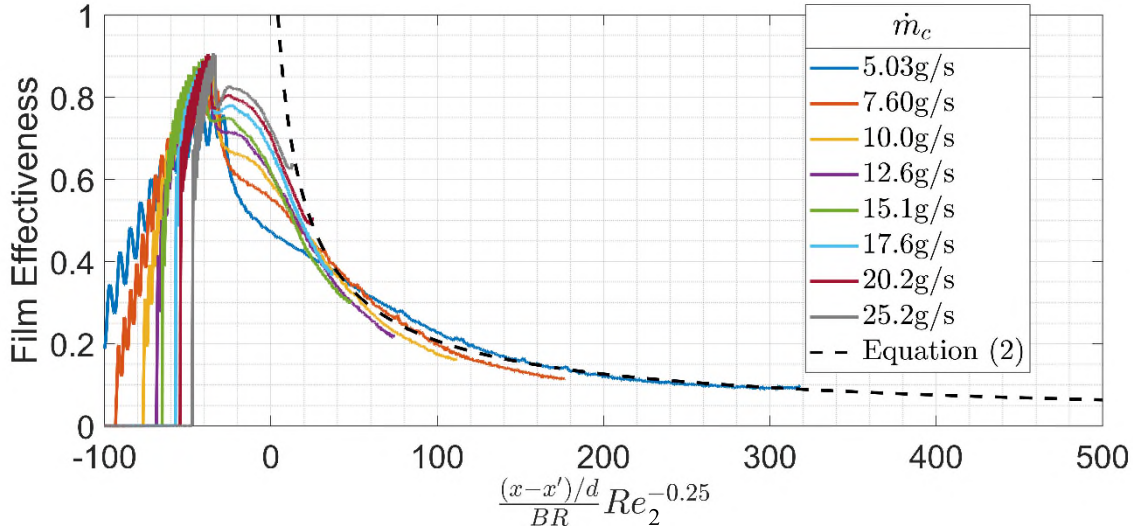

Figure 5 Film effectiveness against scaled streamwise distance with core offset for 17 row inline late suction surface panel (Wambersie, Ireland and Mayo 2021)

2D FILM EFFECTIVENESS CORRELATION

An alternative approach that attempts to capture the 2D distribution of film cooling combines the streamwise term from Equation 7 with the Seller-Goldstein approach of Equation 8 and Equation 9 yielding

$$\eta = \exp\left[-\left(\frac{C_2 hxd}{\dot{m}c_p} + C_1\right)\right] exp\left[-0.693\left(\frac{y}{y_h}\right)^2\right] \tag{10}$$

Where x is the streamwise distance from the film hole and h is defined as the flat plate heat transfer coefficient with mainstream flow conditions defined by those at the film hole exit. The Reynolds number reference length is the distance from the leading edge. Similarly to Equation 7, h serves as an analogy for mixing and heat transfer within the boundary layer.

$$h = 0.0287 P_r^{-0.4} Re^{-0.2} \rho u c_p \tag{11}$$

Two additional parameters, C_1 and C_2 are included. C_1 equates to an offset streamwise distance, whereas C_2 captures the increase in heat transfer due to the disruption in the boundary layer caused by coolant injection. Each film hole is modelled individually and then superimposed using the Sellers superposition approach described by Equation 8. This approach allows for a full 3D film effectiveness distribution starting at the leading edge of the cooling feature to be calculated.

Regression to experimental data

Figure 6 and Figure 7 illustrate the spanwise averaged film effectiveness values calculated using Equation 10 plotted against experimental data in which C_1 and C_2 were selected in order to minimize R^2 for 12 and 13-row geometries on both the suction and pressure surface respectively. The mean R^2 value for these geometries is 0.999 with a maximum deviation in film effectiveness values of 0.03 - well within the range of experimental uncertainty. The main inconsistencies between the model and experimental data lie within the panel and the film holes themselves as the model is unable to predict values measured within the holes.

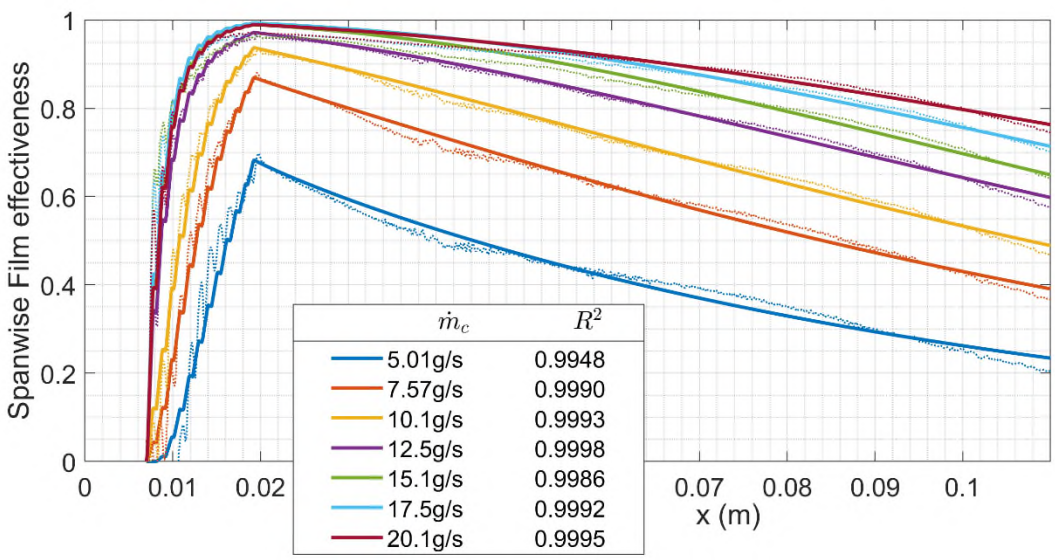

Figure 6 Best fit of Equation 10 (solid line) with experimental film effectiveness data (dotted line) of a 12-row staggered panel geometry located on the early suction surface

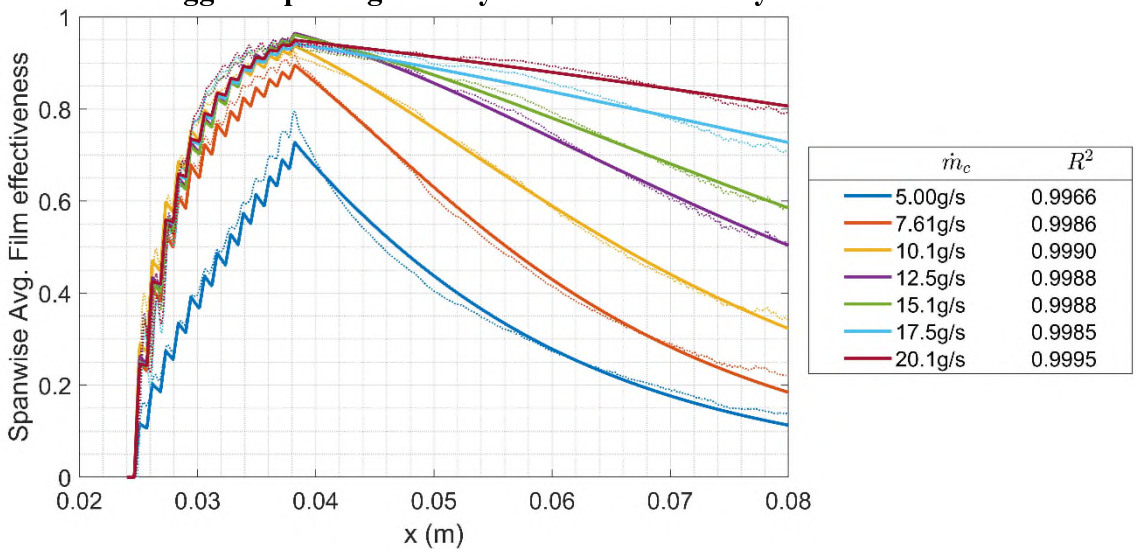

Figure 7 Best fit of Equation 10 (solid line) with experimental film effectiveness data (dotted line) of a 13-row staggered panel geometry located on the mid-pressure surface

The best-fit coefficients C_1 and C_2 for all geometries and mass flows are plotted in Figure 8, with a minimum R^2 value of 0.985 across all geometries. This demonstrates that the form of Equation 10 is able to fit the film effectiveness data very closely with the greatest discrepancies occurring either at very high or very low blowing ratios where partial ingestion or lift-off could be expected.

C_1 is seen to be a strong function of velocity ratio (VR) as variations in coolant density were able to highlight. This indicates that this parameter is driven by the velocity gradient between the film and mainstream. C_1 follows a similar trend for both the suction and pressure surface, with C_1increasing exponentially as VR approaches zero. C_1 is approximately 0.75 for intermediate VRs between 0.5 and 1.5 for both surfaces. When C_1 is a positive value, it can be proposed that the films generated by the high porosity features behave as if stemming from an imaginary tangential slot located $C_1 Mcp/hD$ upstream of the panel.

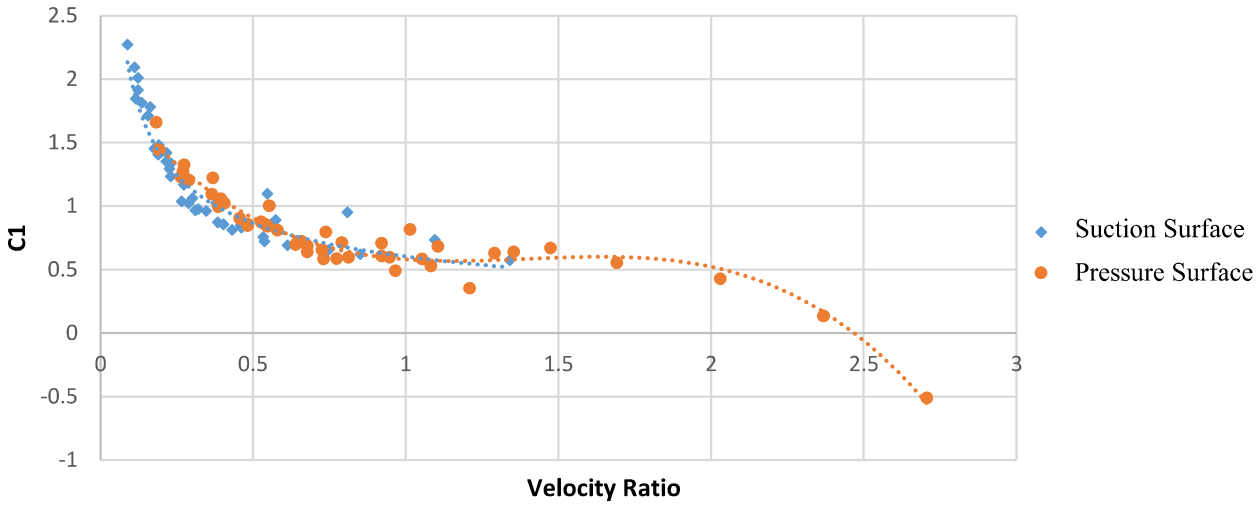

Figure 8 C1 values for the suction and pressure surface geometries against velocity ratio (VR)

C_2 values exhibit greater differences between the suction surface and pressure surface than the C1 levels for a range of BR. C_2 can be considered to capture the effects of coolant injection on the heat transfer coefficient, which in this case serves as a proxy for mixing in the boundary layer. In other words, C_2 acts much like β in Equation 5 and like β would be expected to be a function of blowing ratio. At low blowing ratios, C_2 increases for both surfaces up to a BR of 0.6. As BR is increased further, C_2 on the suction surface continues to increase as the surface curvature enhances the effective angle between the coolant jets and the blade surface. On the pressure surface, however, the concave curvature allows C_2 to recover at moderate BRs as the increased coolant momentum forces it closer to the blade surface. The discrepancy in magnitudes between the two surfaces however remains to be explained and indicates a fundamental difference in the behaviors of the films.

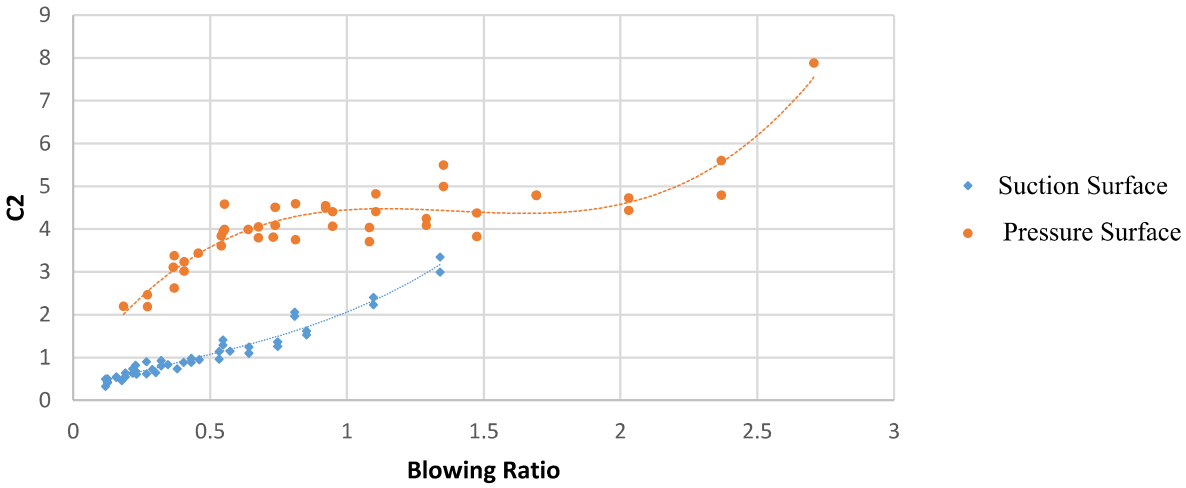

Figure 9 C2 values for suction and pressure surface geometries

GENERAL OBSERVATIONS ON C_1 AND C_2

In order to attempt to find a generalised correlation for all the geometries tested for both surfaces, best fit splines were determined for all of the data and the model is run using values taken from the best fit line. With this approach, an average R^2 value of 0.96 was achieved with values ranging between 0.92 and 0.99. The spread of these values is principally determined by the results at the limits of the range of blowing ratios where ingestion or lift-off may occur.

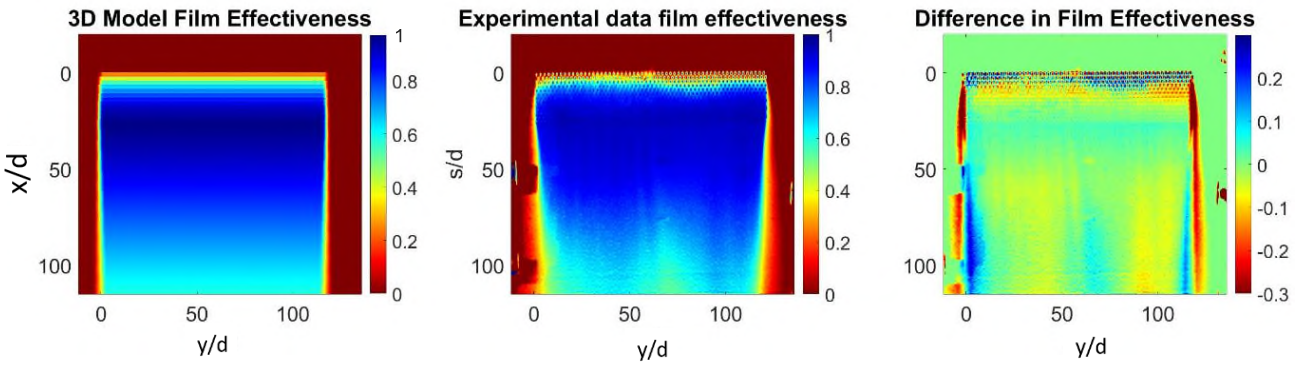

Figure 10 Comparison between film effectiveness levels predicted by correlation and experimental data

Figure 10 plots the full spatial distribution for an example geometry using the curve fitted C_1 and C_2. Comparison between the experiment and model illustrates the high degree of accuracy of the model. The primary discrepancies between the two, highlighted by the rightmost figure are close to the panel edges where the experiment shows a higher degree of spanwise spreading as well as the development of vortices. As previously mentioned, these effects can be captured to some degree by more evolved lateral spreading models. However, with the aim of minimizing complexity and concentrating on the overall bulk of the panel, this task has been left as future work. Minor discrepancies are also noticed between the film holes of the first 4 to 7 rows where the lift-off of individual holes (experimental data) as well as variations in individual film holes is observable. Overall, with the exception of regions dominated by secondary flows, this method proves to be highly successful.

DISCUSSION

A final analysis of the model can be carried out by testing the film effectiveness model on flat plate data taken from another experimental facility. Flat plate data taken from Courtis (Courtis, et al. 2021) was used to generate C_1 and C_2 values in the same manner. These are plotted in Figures 12 and 11 respectively.

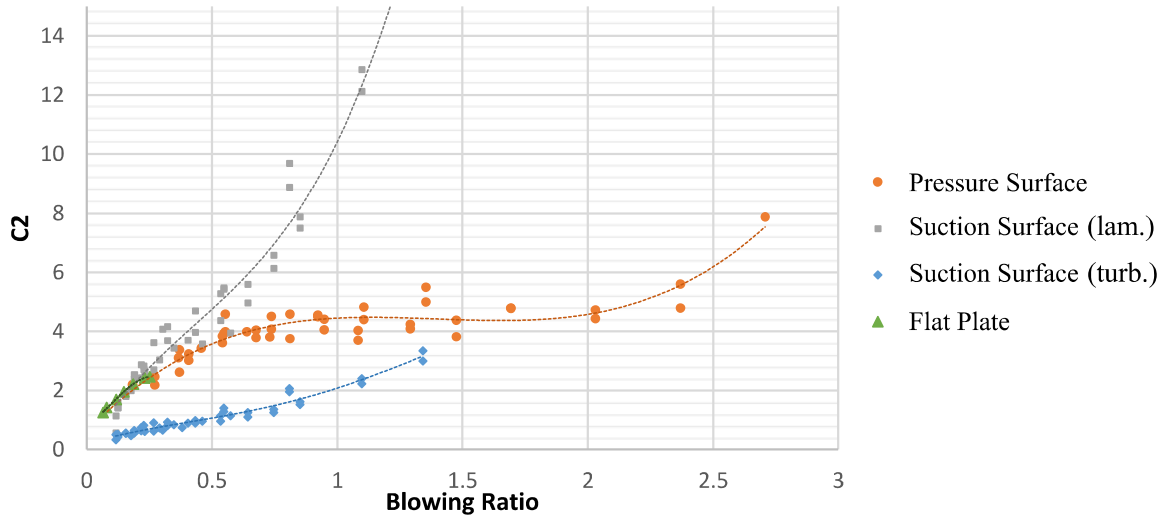

Figure 11 C2 values for equivalent geometries across suction surface, pressure surface and flat plate.

Comparing C_2 values from similar panel geometries in all three setups indicates that both the pressure surface and flat plate exhibit a similar trends with blowing ratio. The data show that the C_2

values for the suction surface are significantly lower than that for the pressure surface at low BRs - approximately one-quarter up to a BR of 0.5. Since C_2 governs the rate at which the film decays with distance, the large difference between the suction surface and the other surfaces offers yet another illustration of how films on the suction surface behave significantly differently from more conventional geometries.

By assuming the suction surface flow is in fact laminar, however, the equation for h can be replaced with a laminar alternative given by Equation 12 and values for C_2 recalculated. Here, a significantly higher value of C_2 is calculated for the suction surface which lines up closely with pressure surface and flat plate values at low blowing ratios. These recalculated values are included in Figure 11 and labelled: Suction Surface (lam.).

$$h_l = 0.332 P_r^{-2/3} Re_{h,x}^{-0.5} \rho_h u_h c_p \tag{12}$$

As the blowing ratio is increased, the effect of curvature becomes more significant and the suction surface films are blown further into the mainstream resulting in more mixing. On the concave surface, the effect is reversed and increased BRs push the film closer to the blade surface, minimizing additional mixing. Overall however, the close agreement between the three surfaces at low BRs indicates that the relaminarization of the flow on the suction surface most likely explains the significant reduction in film degradation. Lastly, when using the laminar assumption on the suction surface, all values of C_2 are calculated to be above unity. This better matches the intended description of C_2 being a penalty incurred due to the film injection into the boundary layer, since if the turbulent assumption of the suction surface boundary layer were maintained, the addition of films would appear to reduce the heat transfer expected within the boundary layer. Refitting C_1values with the new expression for h is also seen to shift the values of C_1 down such that the flat plate lies between the convex surface and concave surfaces indicating a sensitivity to curvature.

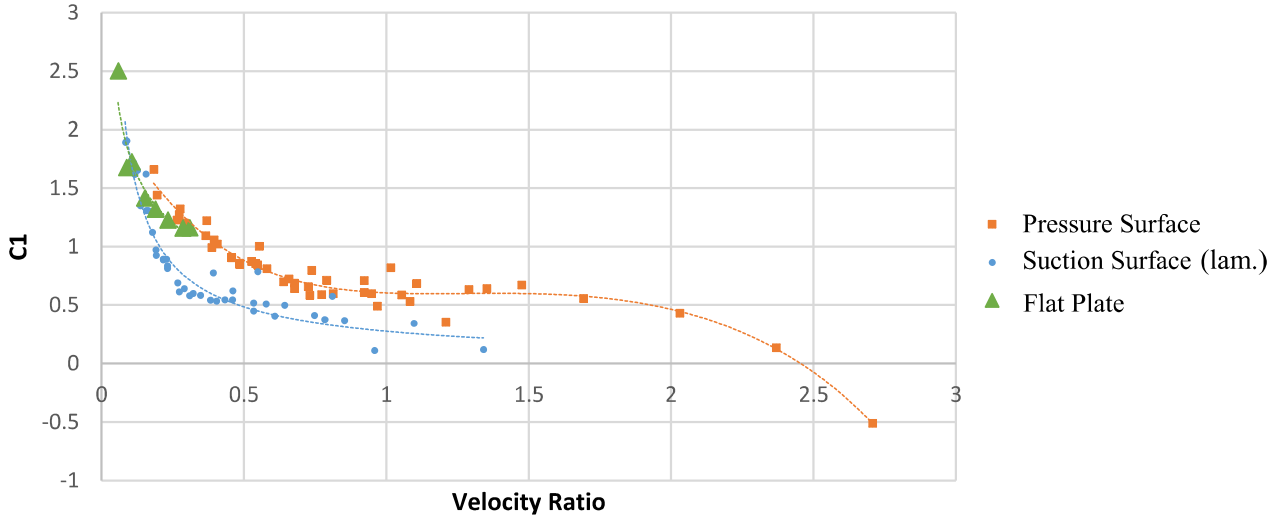

Figure 12 C1 values for flat plate data between pressure surface and laminar suction surface

Whilst a significant assumption to make, the acceleration parameter K on the suction surface is known to exceed values required for relaminarization, between 1 and 3.5x10-6 (Kays and Crawford 1980). Furthermore, the very low blowing ratios and Reynolds numbers within the film cooling holes located at or upstream of this region of strong favorable pressure gradients offer a geometry which minimizes the increase in turbulence within the boundary layer.

CONCLUSIONS

An investigation into the film effectiveness levels of high porosity film cooling features has been carried out. First, it was demonstrated that after a given downstream length, films behave as heat

sinks in a fully mixed out turbulent boundary layer, following the trends of typical 2D film models. However, this region is preceded by a core-like region in which mixing between the mainstream and film coolant is reduced. This core length is increased by reducing individual film hole diameters, blowing ratio, and increasing the overall mass flow.

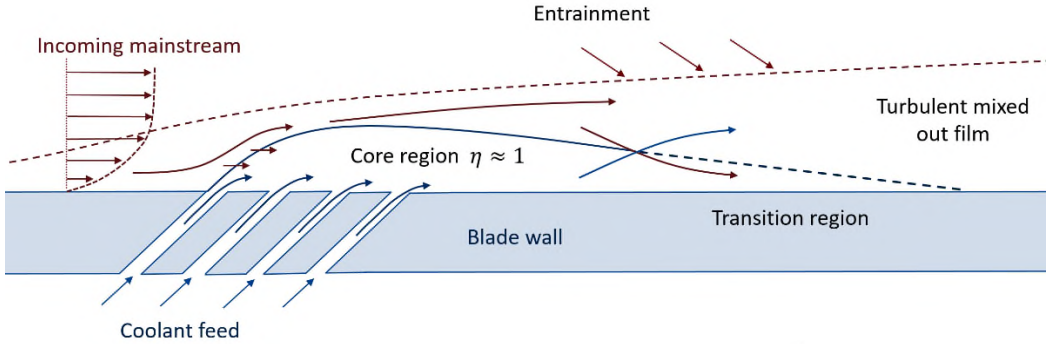

Figure 13 Conceptual model of high porosity films

This results in the significant conclusion that like slot cooling, transpiration cooling does not simply reduce the boundary layer temperature but also acts as a physical barrier between the mainstream and blade surface within the core region.

The correlation proposed was successful in predicting the film effectiveness with a high degree of accuracy as well as with a reasonable level of spatial resolution around the individual film features. Secondary effects are not captured, however, the robustness of these panels means that these effects are mostly insignificant. Again, the model points towards the similarities between the panel geometries, tangential injection slots and transpiration cooling.

Comparing results from both the pressure and suction surface has pointed towards the possibility that low-blowing ratio films on the early suction surface remain in the laminar regime due to the high acceleration parameters potentially explaining the exceptional film effectiveness levels observed.

Extensive work remains to be carried out concerning the investigation of turbulence levels within the suction surface boundary layer as well as the effect of very low BR films being ejected within the region of relaminarization.

The conclusion which can be taken from these modelling approaches lies in the fact that the high porosity panel geometries share the same film cooling trends as both tangential slots and porous sections. Whilst not yet equivalent, the shared trends indicate that the development of transpiration-like cooling features is both achievable and within reach.

ACKNOWLEDGMENTS

The authors wish to express their thanks for the ongoing support provided by both Rolls-Royce PLC and the EPSRC. The authors would also like to thank the technicians at the Oxford Thermofluids Institute for their assistance in the manufacturing of the experimental setup and Dr Matt Courtis for his help with the preparation of Figure 11 and 12.

REFERENCES

Chen, Z, Y Li, X Su, and X. Yuan. 2020. “Accuracy Assessment of the Sellers Model in Predicting the Multi-Row Film Cooling Performance.” *Proceedings of the ASME Turbo Expo 2020: Turbomachinery Technical Conference and Exposition. Volume 7B: Heat Transfer.* Virtual, Online September . V07BT12A010.

Coulton, B., A. V. Murray, and P. Ireland. 2022. “A Computational Approach to Aerothermal Analysis of Complex Internal Turbine Cooling Geometries.” *Proceedings of ASME Turbo Expo 2022: Turbomachinery Technical Conference and Exposition.* Rotterdam: AMSE GT. 81928.

Goldstein, R. J. 1971. "Film Cooling." *Advances in Heat Transfer* (pp. 321-379).

Goldstein, R. J., G. Shavit, and T. S. Chen. 1965. "Film-Cooling Effectiveness With Injection Through a Porous Section." *ASME. J. Heat Transfer. August* 87(3): 353–359.

Hatch, J. E., and S. S. Papell. 1959. "Use of a Theroretical FLow Model to Correlate Data for Film Cooling Or Heating an Adiabatic Wall by Tangential Injection of Gases of Different Fluid Properties." *NASA TN D-130* . November.

Jiang, Y., L. Capone, P. Ireland, and E. Romero. 2018. "A detailed Study of the Interaction Between Two Rows of Cooling Holes." *J. Turbomach.AMSE* 140(4): 041008 (10 pages).

Kirollos, B., and T. Povey. 2015. "An Energy-Based Method for Predicting the Additive Effect of Multiple Film Cooling Rows." *ASME. J. Eng. Gas Turbines Power December* 137(12): 122607.

Murray, A.V., P.T. Ireland, T.H. Wong, S.W. Tang, and A.J Rawlinson. 2018. "High Resolution Experimental and Computational Methods for Modelling Multiple Row Effusion Cooling Performance." *Int. J. Turbomach. Propuls. Power* 3, 4. https://doi.org/10.3390/ijtpp3010004.

Papell, S. S. 1960. "Effect on Gaseous Film Cooling of Coolant Injection Through Angled Slots and Normal Holes." *NASA TN D-299.* September.

Sellers, J. P. 1963. "Gaseous film cooling with multiple injection slots." *AIAA* 1 (9): 2154-2156.

Simon, Frederick F. 1986. "Jet Model for Slot Film Cooling with Effect of Free-Stream and Coolant Turbulence." *Nasa Technical Paper 2655.* NASA, October.

Sturgess, G. J. 1980. "Account of Film Turbulence for Predicting Film Cooling Effectiveness in Gas Turbine Combustors." *ASME. J. Eng. Power. July* 102(3): 524–534.

Sturgess, G. J. 1986. "Design of Combustor Cooling Slots for High Film Effectiveness: Part I—Film General Development." *ASME. J. Eng. Gas Turbines Power. April* 108(2): 354–360.

Wambersie, Augustin, Peter Ireland, and Ignacio Mayo. 2021. "Experiments of Transpiration Cooling Inspired Panel Cooling on a Turbine Blade Yielding Film Effectiveness Levels over 95%." *Int. J. Turbomach. Propuls. Power* 6(2), 16.

